10.48047/jocaaa.2020.28.06.18

Axisymmetric Dual-Phase-Lag Thermoelastic Diffusion under Coupled Thermodiffusive Sources

Sandeep Kumar[1] and Rajneesh Kumar[2]
[1]Department of Mathematics, Chaudhary Devi Lal University, Sirsa, Haryana, India
[2]Department of Mathematics, Kurukshetra University, Kurukshetra, Haryana, India
Corresponding Author 1goyat_sandeep30@yahoo.com, 2rajneesh_kuk@rediffmail.com

Abstract

The purpose of this paper is to study the effects of thermal and diffusion phase lags due to axisymmetric heat supply in a ring. The problem is formulated within the framework of dual-phase-lag heat transfer (DPLT) and dual-phase-lag diffusion (DPLD) models. The upper and lower surfaces of the ring are traction-free and subjected to an axisymmetric heat supply. The solution is obtained using Laplace and Hankel transform techniques. Analytical expressions for displacement, stresses, chemical potential, temperature, and mass concentration are obtained in the transformed domain. A numerical inversion technique is applied to recover the results in the physical domain. The numerically simulated results are presented graphically. The effects of thermal and diffusion phase lags on various field quantities are discussed. Some particular cases are also deduced from the present investigation. The results obtained may be useful in analysing axisymmetric thermodiffusive responses in geophysical, material-processing, and industrial systems involving coupled thermal and mass diffusion effects.

Keywords: Thermoelastic diffusion; Dual phase lags; Laplace Transform; Hankel Transform; Axisymmetric problem.

1. Introduction

Classical Fourier heat-conduction theory assumes that a thermal disturbance propagates with infinite speed, which is physically unrealistic in problems involving short time scales, small dimensions, rapid heating, and high-frequency thermal loading. This limitation becomes particularly important in generalized thermoelasticity, where thermal, mechanical, and diffusive fields interact with one another. To remove the paradox of infinite thermal-wave speed, Lord and Shulman [1] introduced a generalized thermoelasticity theory by incorporating a thermal relaxation time into the heat-conduction equation. In this single-relaxation-time model, the heat flux does not respond instantaneously to changes in the temperature field, and thermal waves propagate with finite speed when the relaxation time is non-zero. Green and Lindsay [2] further extended this framework by introducing two distinct relaxation parameters associated with the temperature and stress fields, thereby providing greater flexibility in modelling thermoelastic responses.

A more general description of non-Fourier heat transport was later proposed by Tzou [3], who introduced the dual-phase-lag heat-conduction model. In this model, two distinct delay times are considered: the phase lag of the heat flux and the phase lag of the temperature gradient. The heat-flux phase lag represents the delay caused by thermal inertia during fast transient processes, whereas the temperature-gradient phase lag accounts for the delay associated with microstructural interactions. This formulation provides a bridge between microscopic and macroscopic heat-transfer descriptions and includes several classical and generalized heat-conduction models as special cases. Quintanilla and Racke [4] investigated stability aspects of dual-phase-lag heat conduction and compared mathematical hyperbolic formulations associated with this model. Rukolaine [5] later discussed possible unphysical effects of the dual-phase-lag

10.48047/jocaaa.2020.28.06.18

model, emphasizing the need for careful selection of phase-lag parameters and thermodynamically consistent formulations.

The dual-phase-lag model has been applied to several thermal and thermoelastic problems involving rapid heating, layered media, laser irradiation, and wave propagation. Abdallah [6] used an uncoupled thermoelastic model based on the dual-phase-lag theory to study the thermoelastic response of a semi-infinite medium subjected to ultrashort pulsed laser heating. Chou and Yang [7] analysed two-dimensional dual-phase-lag thermal behaviour in single-layer and multilayer structures using the conservation-element and solution-element method. Zhou, Zhang and Chen [8] proposed an axisymmetric dual-phase-lag bioheat model for laser heating of living tissues, demonstrating the applicability of phase-lag heat conduction in cylindrical and axisymmetric configurations. Liu, Cheng and Wang [9] analysed thermal damage in a laser-irradiated tissue based on a non-Fourier heat-conduction model. Ying and Yun [10] developed a time-fractional dual-phase-lag heat-conduction equation and the corresponding bioheat-transfer formulation, extending phase-lag theory to fractional-order heat-transport processes.

In thermoelastic media, phase-lag effects significantly influence wave propagation, deformation, and stress distributions. Kumar and Mukhopadhyay [11] investigated the propagation of harmonic waves in thermoelastic media using a theory involving three phase lags. Kumar, Chawla and Abbas [12] examined the effect of viscosity on wave propagation in an anisotropic thermoelastic medium under the three-phase-lag model. Sharma, Sharma and Bhargava [13] studied the role of viscosity in thermoelasticity and showed that dissipative effects can strongly modify thermoelastic responses. Sharma, Sharma and Bhargava [14] further analysed wave motion in electro-microstretch solids, contributing to the understanding of wave propagation in complex continua. Sharma and Kumar [15] investigated plane waves in a thermoviscoelastic medium. Sharma and Bhargava [16] studied thermoelastic plane waves at an imperfect boundary, showing the influence of boundary imperfections on reflected and transmitted waves.

Thermoelastic diffusion theory provides a framework for analysing the interaction of thermal, elastic, and mass-diffusion fields. Diffusion is the spontaneous transport of particles from a region of higher concentration to a region of lower concentration under the influence of a concentration gradient. In elastic solids, thermodiffusion arises from the coupling among temperature, strain, mass concentration, and chemical potential. Nowacki [17] first developed the theory of thermoelasticity with mass diffusion within the coupled thermoelastic framework; however, this formulation retains the classical limitation of infinite propagation speeds for thermoelastic waves. Sherief, Saleh and Hamza [18] developed the theory of generalized thermoelastic diffusion, which predicts finite speeds of propagation for both thermoelastic and diffusive waves. Kumar and Kansal [19] derived the basic equations of generalized thermoelastic diffusion in the Green–Lindsay framework and investigated Lamb-wave propagation in a transversely isotropic thermoelastic diffusion plate. Sharma [20] studied boundary-value problems in generalized thermodiffusive elastic media and highlighted the importance of diffusion effects in coupled deformation problems. Sharma [21] analysed deformation due to an inclined load in a generalized thermodiffusive elastic medium. Sharma, Kumar and Ram [22] investigated interactions in generalized thermoelastic diffusion caused by inclined loading, further establishing the relevance of diffusion effects in mechanically loaded thermoelastic solids.

Several authors have extended thermoelastic diffusion theory by incorporating additional physical mechanisms such as fractional parameters, two-temperature effects, variable transport properties, and phase-lag diffusion. Atwa [23] studied generalized thermoelastic diffusion with the effect of a fractional parameter on plane waves in a temperature-dependent elastic medium. Bhattacharya and Kanoria [24] investigated elasto-thermo-diffusion inside a spherical shell under the influence of two-temperature generalized thermoelasticity. Kumar and Gupta [25] considered plane-wave propagation in an anisotropic dual-phase-lag thermoelastic diffusion medium and introduced phase-lag effects into the diffusion process. Tripathi, Kedar and Deshmukh [26] analysed a generalized thermoelastic diffusion problem in a thick circular plate subjected to axisymmetric heat supply, showing the significance of axisymmetric thermal loading in diffusive thermoelastic media. Li, Guo, Tian and Tian [27] studied the transient response of a half-space with variable thermal conductivity and diffusivity under thermal and chemical

10.48047/jocaaa.2020.28.06.18

shock, demonstrating that variable transport properties can strongly influence thermal and diffusive waves. Kumar, Miglani and Rani [28] investigated a two-dimensional axisymmetric thermoelastic diffusion problem for a micropolar porous circular plate using the dual-phase-lag model. Xue, Yu, Li and Tian [29] examined a generalized thermoelastic diffusion bi-layered structure with variable thermal conductivity and diffusivity. Tokovyy [30] presented solutions of axisymmetric elasticity and thermoelasticity problems for inhomogeneous spaces and half-spaces, which are relevant to the mathematical treatment of axisymmetric thermoelastic configurations.

Despite extensive work on generalized thermoelasticity, dual-phase-lag heat conduction, and thermoelastic diffusion, the coupled axisymmetric response under simultaneous thermal excitation and ring-type diffusive source has received limited attention. This gap is significant for transient processes in which both heat flux and diffusing mass flux exhibit delayed responses. Motivated by this, the present study formulates an axisymmetric dual-lag thermoelastic diffusion problem for a homogeneous isotropic medium subjected to coupled thermodiffusive sources. Using Laplace and Hankel transforms, expressions for displacement, stresses, temperature change, chemical potential, and mass concentration are obtained in the transformed domain. The influence of thermal and diffusion phase lags is analysed numerically, and relevant classical and generalized models are recovered as limiting cases.

2. Basic Equations

The basic equations of motion, heat conduction and mass diffusion in a homogeneous isotropic thermoelastic solid with DPLT and DPLD models in the absence of body forces, heat sources and mass diffusion sources are followed from the work of [25]

$$(\lambda+\mu)\nabla(\nabla.u)+\mu\nabla^2 u-\beta_1\nabla T-\beta_2\nabla C=\rho\ddot{u} \tag{1}$$

$$\left(1+\tau_t\frac{\partial}{\partial t}\right)KT_{,ii}=\left(1+\tau_q\frac{\partial}{\partial t}+{\tau_q}^2\frac{\partial^2}{\partial t^2}\right)[\rho C_E\dot{T}+\beta_1 T_0\dot{e}_{kk}+aT_0\dot{C}] \tag{2}$$

$$\left(1+\tau_p\frac{\partial}{\partial t}\right)(D\beta_2\nabla^2(\nabla.u)+Da\nabla^2 T-Db\nabla^2 C)+\frac{\partial}{\partial t}\left(1+\tau_\eta\frac{\partial}{\partial t}+{\tau_\eta}^2\frac{\partial^2}{\partial t^2}\right)C=0 \tag{3}$$

and the constitutive relations are

$$\sigma_{ij}=2\mu e_{ij}+\delta_{ij}(\lambda e_{kk}-\beta_1 T-\beta_2 C) \tag{4}$$

$$\rho T_0 S=\left(1+\tau_q\frac{\partial}{\partial t}+{\tau_q}^2\frac{\partial^2}{\partial t^2}\right)(\rho C_E T+\beta_1 T_0 e_{kk}+aT_0 C) \tag{5}$$

$$P=-\beta_2 e_{kk}-aT-bC \tag{6}$$

Where λ , μ are Lame's constants , ρ is the density assumed to be independent of time, D is the diffusivity, P is the chemical potential per unit mass, C is the concentration, u_i are components of displacement vector u, K is the coefficient of thermal conductivity, C_E is the specific heat at constant strain, $T=\vartheta-T_0$ is small temperature increment, ϑ is the absolute temperature of the medium, T_0 is the reference temperature of the body such that $\left|\frac{T}{T_0}\right|\ll 1$, a and b are respectively , the coefficients describing the measure of thermodiffusion and mass diffusion effect respectively, σ_{ij} and e_{ij} are the components of stress and strain respectively, e_{kk} is dilatation, S is the entropy per unit mass, $\beta_1=(3\lambda+2\mu)\alpha_t$ $\beta_2=(3\lambda+2\mu)\alpha_c$, α_c is the coefficient of linear diffusion expansion and α_t is the coefficient of thermal linear expansion. τ_t, τ_q, τ_p, τ_η are respectively phase lag of temperature gradient, the phase lag of heat flux, the phase lag of chemical potential, and phase lag of diffusing mass flux vector. In above

10.48047/jocaaa.2020.28.06.18

equations, a comma followed by suffix denotes spatial derivative and a superposed dot denotes derivative with respect to time.

3. Formulation and Solution of the Problem

Consider a homogeneous isotropic, generalized thermoelastic diffusion thick plate of thickness $2b_1$ defined by $0 \le r \le \infty$, $-b_1 \le z \le b_1$. Cylindrical polar coordinates (r, ϕ, z) having origin on the surface $z = 0$, between the lower and upper surfaces of the plate and the z-axis is assumed to be the axis of symmetry. Due to symmetry about z-axis all the field quantities depending only on (r, z, t). The initial temperature in the thick plate is given by a constant temperature T_0 and the heat flux $g_0 F(r, z)$ is prescribed on the upper and lower boundary surfaces. We consider chemical potential source (ring source) which emanates from the origin of the coordinates and expands radically at constant rate c over the surface. Under these conditions, thermoelastic quantities in a semi-infinite thick circular plate are required to be determined. As the problem considered is plane axisymmetric, the field component $u_\theta = 0$, and u_r, u_z, T and C are independent of θ and restrict our analysis to the two dimensional problem with

$$\boldsymbol{u} = (u_r, 0, u_z) \tag{7}$$

Equations (1)-(6) with the aid of (7) take the form

$$(\lambda + \mu)\frac{\partial e}{\partial r} + \mu\left(\nabla^2 - \frac{1}{r^2}\right)u_r - \beta_1\frac{\partial T}{\partial r} - \beta_2\frac{\partial C}{\partial r} = \rho\frac{\partial^2 u_r}{\partial t^2} \tag{8}$$

$$(\lambda + \mu)\frac{\partial e}{\partial z} + \mu\nabla^2 u_z - \beta_1\frac{\partial T}{\partial z} - \beta_2\frac{\partial C}{\partial z} = \rho\frac{\partial^2 u_z}{\partial t^2} \tag{9}$$

$$(1+\tau_t\frac{\partial}{\partial t})\mathrm{K}\nabla^2 T = \left(1 + \tau_q\frac{\partial}{\partial t} + \frac{{\tau_q}^2}{2}\frac{\partial^2}{\partial t^2}\right)[\rho C_E\dot{T} + \beta_1 T_0\frac{\partial}{\partial t}div\, u + aT_0\frac{\partial C}{\partial t}] \tag{10}$$

$$(1+\tau_p\frac{\partial}{\partial t})(D\beta_2\nabla^2 div\, u + Da\nabla^2 T - Db\nabla^2 C) + \frac{\partial}{\partial t}\left(1 + \tau_\eta\frac{\partial}{\partial t} + \frac{{\tau_\eta}^2}{2}\frac{\partial^2}{\partial t^2}\right)C = 0 \tag{11}$$

and Constitutive relations

$$\sigma_{rr} = 2\mu e_{rr} + \lambda e - \beta_1 T - \beta_2 C \tag{12}$$

$$\sigma_{\theta\theta} = 2\mu e_{\theta\theta} + \lambda e - \beta_1 T - \beta_2 \tag{13}$$

$$\sigma_{zz} = 2\mu e_{zz} + \lambda e - \beta_1 T - \beta_2 C \tag{14}$$

$$\sigma_{rz} = \mu e_{rz}\, ,\, \sigma_{r\theta} = 0\, ,\, \sigma_{z\theta} = 0 \tag{15}$$

$$P = -\beta_2 e - aT + bC \tag{16}$$

$$\text{where} = \frac{\partial u_r}{\partial r} + \frac{u_r}{r} + \frac{\partial u_z}{\partial z}\, ,\, e_{rr} = \frac{\partial u_r}{\partial r}\, ,\quad e_{\theta\theta} = \frac{u_r}{r}\, ,\, e_{zz} = \frac{\partial u_z}{\partial z}\, ,\, e_{rz} = \frac{1}{2}\left(\frac{\partial u_r}{\partial z} + \frac{\partial u_z}{\partial r}\right) \tag{17}$$

To facilitate the solution, the following dimensionless quantities are introduced

$$r' = \frac{\omega_1^*}{c_1}r\, ,\, z' = \frac{\omega_1^*}{c_1}z\, ,\, (u_r', u_z') = \frac{\omega_1^*}{c_1}(u_r, u_z),\, t' = \omega_1^* t\, ,\, (\sigma_{rr}', \sigma_{\theta\theta}', \sigma_{zz}', \sigma_{rz}') = \frac{1}{\beta_1 T_0}(\sigma_{rr}, \sigma_{\theta\theta}, \sigma_{zz}, \sigma_{rz})$$

10.48047/jocaaa.2020.28.06.18

$$(T', C') = \frac{\beta_1}{\rho c_1^2}(T, C)\ ,\ \ (\tau_q', \tau_t', \tau_p', \tau_\eta') = \omega_1^*(\tau_q, \tau_t, \tau_p, \tau_\eta)\ ,\ \omega_1^* = \frac{\rho C_E c_1^2}{K}\ ,\ c_1^2 = \frac{\lambda+2\mu}{\rho} \tag{18}$$

We define Laplace and Hankel transforms as:

$$\bar{f}(r, z, s) = \int_0^\infty f(r, z, t) e^{-st} dt \tag{19}$$

$$\hat{f}(\xi, z, s) = \int_0^\infty \bar{f}(r, z, s) r J_n(r\xi)\, dr \tag{20}$$

Using (18) in equations (8)-(11), suppressing the primes, and then applying the Laplace transform defined by (19) on the resulting equations yield

$$\nabla^2 \bar{T} + \nabla^2 \bar{C} - (\nabla^2 - s^2)\bar{e} = 0 \tag{21}$$

$$(\nabla^2 - \frac{\tau_q^1}{\tau_t'} ks)\bar{T} - \frac{K a T_0 \tau_q^1 s}{\rho C_E \beta_2 \tau_t'} \bar{C} - \frac{K {\beta_1}^2 T_0}{\rho^2 C_E c_1^2} \frac{\tau_q^1}{\tau_t'} s\, \bar{e} = 0 \tag{22}$$

$$Da \nabla^2 \frac{\rho c_1^2}{\beta_1} \bar{T} - \left(Db \frac{\rho c_1^2}{\beta_2} \nabla^2 - \frac{s \tau_\eta' k c_1^2}{\tau_p' \beta_2 C_E} \right) \bar{C} + D\beta_2 \nabla^2 \bar{e} = 0 \tag{23}$$

where $\tau_q^1 = 1 + s\tau_q + \frac{s^2 {\tau_q}^2}{2}$, $\tau_\eta^1 = 1 + s\tau_\eta + \frac{s^2 {\tau_\eta}^2}{2}$, $\tau_p^1 = 1 + s\tau_p$, $\tau_t^1 = 1 + s\tau_t$

Eliminating $\bar{T}$, $\bar{C}$, $\bar{e}$ from equations (21)-(23), we obtain

$$(\nabla^2 - k_1^2)(\nabla^2 - k_2^2)(\nabla^2 - k_3^2)(\bar{T}, \bar{C}, \bar{e}) = 0 \tag{24}$$

The solutions of the equation (24) can be written in the form

$$\bar{T} = \sum_{i=1}^3 \bar{T}_i\ ,\ \bar{e} = \sum_{i=1}^3 \bar{e}_i\ ,\ \bar{C} = \sum_{i=1}^3 \bar{C}_i \tag{25}$$

where $\bar{T}_i$, $\bar{e}_i$,and $\bar{C}_i$ are solutions of the following equation

$$(\nabla^2 - k_i^2)(\bar{T}_i, \bar{e}_i, \bar{C}_i) = 0\ ,\ i = 1,2,3 \tag{26}$$

On taking Hankel transform defined by (20) on (25) and (26), we obtain

$$\hat{T} = \sum_{i=1}^3 \hat{T}_i\ ,\ \ \hat{e} = \sum_{i=1}^3 \hat{e}_i,\ \ \hat{C} = \sum_{i=1}^3 \hat{C}_i$$

$$\left(D^2 - \xi^2 - k_i^2\right)(\hat{T}_i, \hat{e}_i, \hat{C}_i) = 0\ \ , \tag{27}$$

Therefor, the solution of equqtion (27), gives

$$\hat{T} = = \sum_{i=1}^3 A_i \cosh(q_i z) \tag{28}$$

$$\hat{C} = \sum_{i=1}^3 g_i A_i \cosh(q_i z) \tag{29}$$

$$\hat{e} = \sum_{i=1}^3 h_i A_i \cosh(q_i z) \tag{30}$$

where,

10.48047/jocaaa.2020.28.06.18

$g_i = \frac{\zeta_{33}q_i^4 - 6)\zeta_{21}\zeta_{33}q_i^2 + \zeta_{23}\zeta_{31}}{-q_i^2(\zeta_{22}\zeta_{33}+\zeta_{23}\zeta_{32})+\zeta_{23}\zeta'_{32}}$

$h_i = \frac{-\zeta_{32}q_i^4 + (\zeta'_{32}+\zeta_{21}\zeta_{32})q_i^2 - \zeta_{21}\zeta'_{32}}{-q_i^2(\zeta_{22}\zeta_{33}+\zeta_{23}\zeta_{32})+\zeta_{23}\zeta'_{32}}$

$q_i = \sqrt{\xi^2 + k_i^2}\,,\ \zeta_{21} = \frac{\tau_q^1}{\tau_t^1} ks\,,\ \zeta_{22} = \frac{KaT_0\tau_q^1 s}{\rho C_E \beta_2 \tau_t^1}\,,\ \zeta_{23} = \frac{K{\beta_1}^2 T_0}{\rho^2 C_E c_1^2}\frac{\tau_q^1}{\tau_t^1} s\,,\ \zeta_{31} = \frac{Da\rho c_1^2}{\beta_1}\,,$

$\zeta_{32} = Db\frac{\rho c_1^2}{\beta_2}\,,\ \zeta_{32}^1 = \frac{s\tau_\eta^1 k c_1^2}{\tau_p^1 \beta_2 C_E}\ ,\ \zeta_{33} = D\beta_2$

Applying inversion of Hankel transform on (28)-(30), we get

$$\bar{T} = \int_0^\infty \{\textstyle\sum_{i=1}^3 A_i \cosh(q_i z)\}\xi J_0(\xi r) d\xi \tag{31}$$

$$\bar{C} = \int_0^\infty \{\textstyle\sum_{i=1}^3 g_i A_i \cosh(q_i z)\}\xi J_0(\xi r) d\xi \tag{32}$$

$$\bar{e} = \int_0^\infty \{\textstyle\sum_{i=1}^3 h_i A_i \cosh(q_i z)\}\xi J_0(\xi r) d\xi \tag{33}$$

Using (8)-(11), (18) and (31)-(33), we obtain the displacement components in the transformed domain as

$$\bar{u}_r(r,z,s) = \int_0^\infty \xi^2 J_1(\xi r)\left[E(\xi,s)\cosh(qz) + \sum_{i=1}^3 \frac{\lambda_i}{\left(\frac{\mu q_i^2}{\rho c_1^2} - s^2\right)}\cosh(q_i z)\right] d\xi \tag{34}$$

$$\bar{u}_z(r,z,s) = \int_0^\infty \xi J_0(\xi r)\left[F(\xi,s)\sinh(qz) - \sum_{i=1}^3 \frac{\lambda_i}{\left(\frac{\mu q_i^2}{\rho c_1^2} - s^2\right)}\sinh(q_i z)\right] d\xi \tag{35}$$

where

$\lambda_i = \left(\frac{\lambda+\mu}{\rho c_1^2} h_i - 1 - g_i\right) A_i\ ,\ \ F(\xi,s) = \frac{\xi^2 E(\xi,s)}{q}\,,\ q = \sqrt{\xi^2 + \frac{\rho c_1^2}{\mu} s^2}$

Substituting the values of (31)-(35) in (12)-(15) and with the aid of (18) yield

$$\overline{\sigma_{\theta\theta}} = \frac{2\mu}{\beta_1 T_0}\int_0^\infty \xi^2 J_1(\xi r)\left[E(\xi,s)\cosh(qz) + \sum_{i=1}^3 \frac{\lambda_i}{\left(\frac{\mu q_i^2}{\rho c_1^2} - s^2\right)}\cosh(q_i z)\right] d\xi\ + \int_0^\infty \sum_{i=1}^3 \eta_i \cosh(q_i z)\, \xi J_0(\xi r)\ d\xi \tag{36}$$

$$\overline{\sigma_{rr}} = \frac{2\mu}{\beta_1 T_0}\int_0^\infty \xi^3 \left(\frac{1}{\xi r} J_1(\xi r) - J_0(\xi r)\right)\left[E(\xi,s)\cosh(q_i z) + \sum_{i=1}^3 \frac{\lambda_i}{\left(\frac{\mu q_i^2}{\rho c_1^2} - s^2\right)}\cosh(q_i z)\right] d\xi + \int_0^\infty \sum_{i=1}^3 \eta_i \cosh(q_i z)\, \xi J_0(\xi r)\ d\xi \tag{37}$$

10.48047/jocaaa.2020.28.06.18

$$\overline{\sigma_{zz}} = \frac{2\mu}{\beta_1 T_0}\int_0^\infty \xi J_0(\xi r)\left[F(\xi,s)q\cosh(qz) + \sum_{i=1}^{3}\frac{\lambda_i q_i^2}{\left(\frac{\mu q_i^2}{\rho c_1^2} - s^2\right)}\cosh(q_i z)\right]d\xi +$$

$$\int_0^\infty \sum_{i=1}^{3}\eta_i \cosh(q_i z)\,\xi J_0(\xi r)\ d\xi \tag{38}$$

$$\overline{\sigma_{rz}} = \frac{\mu}{2\beta_1 T_0}\int_0^\infty \xi^2 J_1(\xi r)\left[\left(\frac{q^2-\xi^2}{q}\right)E(\xi,s)\,\mathrm{q}\sinh(qz) + 2\sum_{i=1}^{3}\frac{\lambda_i}{\left(\frac{\mu q_i^2}{\rho c_1^2} - s^2\right)} q_i \sinh(q_i z)\right]d\xi \tag{39}$$

$$\bar{P}(r,z,s) = \int_0^\infty \sum_{i=1}^{3}\zeta_i \cosh(q_i z)\,\xi J_0(\xi r)\ d\xi \tag{40}$$

where $\eta_i = \left(\frac{f_i - \rho c_1^2 - \rho c_1^2 g_i}{\beta_1 T_0}\right)A_i$, $F(\xi,s) = \frac{\xi^2(E(\xi,s)}{q}$, $\zeta_i = \left(-\beta_2 h_i - \frac{\rho c_1^2}{\beta_1} + \frac{b\rho c_1^2}{\beta_2}\ g_i\right)A_i$

4. Boundary Conditions

At the stress-free surfaces $z = \pm b_1$, the plate is subjected to an axisymmetric thermal source and a ring-type chemical potential source of unit magnitude. The normal and shear stress components are assumed to vanish on these surfaces. Thus, the boundary conditions are prescribed as

$$\frac{\partial T}{\partial z} = \pm g_0 F(r,z), \tag{41}$$

$$\sigma_{zz} = 0, \tag{42}$$

$$\sigma_{rz} = 0, \tag{43}$$

$$P = f(r,t) \tag{44}$$

Where

$$F(r,z) = z^2 e^{-\omega r} \tag{45}$$

$$f(r,t) = \frac{1}{2\pi r}\delta(ct - r) \tag{46}$$

and g_0 is constant temperature applied on the boundary, $\delta(\,)$ is Dirac delta function, c is constant

Applying the Laplace and the Hankel transforms given by (19) and (20) to the boundary conditions (41)–(44), we obtain

$$\frac{d\hat{T}}{dz} = g_0 \hat{F}(\xi\,,z) \tag{47}$$

$$\widehat{\sigma_{zz}} = 0 \tag{48}$$

$$\widehat{\sigma_{rz}} = 0 \tag{49}$$

$$\hat{P} = \hat{f}(\xi,s) \tag{50}$$

10.48047/jocaaa.2020.28.06.18

The transformed thermal and chemical potential source functions are given by

$$\hat{F}(\xi, s) = \frac{z^2\omega}{(\omega^2+\alpha^2)^{3/2}}, \tag{51}$$

$$\hat{f}(\xi, s) = \frac{1}{2\pi}\frac{1}{\sqrt{(\eta^2c^2+s^2)}} \tag{52}$$

Substitute the values of $\bar{T}$, $\overline{\sigma_{zz}}$, $\overline{\sigma_{rz}}$, $\bar{P}$ in (47)-(50), we obtain the values of unknown parameters as

$$A_1 = \frac{\Delta_1}{\Delta}, A_2 = \frac{\Delta_2}{\Delta}, A_3 = \frac{\Delta_3}{\Delta}, E(\xi, s) = \frac{\Delta_4}{\Delta} \tag{53}$$

where

$$\Delta = \begin{vmatrix} \Delta_{11} & \Delta_{12} & \Delta_{13} & 0 \\ \Delta_{21} & \Delta_{22} & \Delta_{23} & \dfrac{-2\mu}{\beta_1 T_0}\xi^2 q cos(qb_1) \\ \Delta_{31} & \Delta_{32} & \Delta_{33} & \dfrac{q^2-\xi^2}{q}\sinh(qb_1) \\ \Delta_{41} & \Delta_{42} & \Delta_{43} & 0 \end{vmatrix}$$

$\Delta_{1i} = q_i \sinh(q_i b_1)$, $\Delta_{2i} = (\mu_i q_i^2 + \eta_i)\cosh(q_i b_1)$, $\Delta_{3i} = \mu_i q_i \sinh(q_i b_1)$, $\Delta_{4i} = \zeta_i \cosh(q_i b_1)$, i=1,2,3 and Δ_i is obtained from Δ, by interchanging i^{th} column with $\left[g_0 F(\xi, b_1) \;\; 0 \;\; 0 \;\; \frac{1}{2\pi}\frac{1}{\sqrt{(\eta^2c^2+s^2)}}\right]^{t_r}$, where t_r denotes transpose.

5. Inversion of Transforms

Due to the complexity of the solution in the Laplace transform domain, the inverse of the Laplace transform is obtained by using the Gaver–Stehfest algorithm. Gaver [31] and Stehfest [32,33] derived the formula given below. By this method, the inverse $f(t)$ of Laplace transform $\bar{f}(s)$ is approximated by

$$f(t) = \frac{log2}{t}\sum_{j=1}^{k} D(j, K)F\left(j\frac{log2}{t}\right)$$

with

$$D(j, K) = (-1)^{j+M}\sum_{n=m}^{\min(j,M)}\frac{n^M(2n)!}{(M-n)!n!(n-1)!(j-n)!(2n-j)!}$$

Where *K* is an even integer, whose value depends on the word length of computer used. *M=K/2,* and *m* is an integer part of $(j+1)/2$. The optimal value of K was chosen as described in Gaver-Stehfast algorithm, for the fast convergence of results with desired accuracy. The Romberg numerical integration technique [34] with variable step size was used to evaluate the results involved.

6. Particular Cases

10.48047/jocaaa.2020.28.06.18

(i) Neglecting the diffusion effect, i.e $\beta_2, a, b = 0$, the expressions reduce to those for displacement components, stresses, and temperature distribution in a thermoelastic isotropic half-space.

(ii) Setting $\tau_t = \tau_q = \tau_\eta = \tau_p = 0$ in equations (39)-(40), together with equations (51)–(53), gives the corresponding expressions for the classical thermoelastic diffusion model.

(iii) Taking $\tau_p = \tau_\eta = 0$ in equations (39)-(40), together with equations (51)–(53), yields the corresponding expressions for the dual-phase-lag heat transfer (DPLT) model.

(iv) Setting $\tau_q = 0$ and $\tau_p = 0$ in equations (39)-(40), together with equations (51)-(53), gives the corresponding expressions for the single-phase-lag heat transfer (SPLT) and single-phase-lag diffusion (SPLD) models.

7. Numerical Results and Discussion

For numerical computation, the mathematical model is evaluated using copper as the material. The material constants are taken from Dhaliwal and Singh [35]:

$\lambda = 7.76 \times 10^{10} Nm^{-2}$, $\mu = 3.86 \times 10^{10} Nm^{-2}$, $K = 386 JK^{-1}m^{-1}s^{-1}$, $\beta_1 = 5.518 \times 10^6\ Nm^{-2}deg^{-1}$, $\rho = 8954\ Kgm^{-3}$, $a = 1.2\ \times 10^4 m^2/s^2 k$, $b = 0.9\ \times 10^6 m^5/kgs^2$, $D = 0.88\ \times 10^{-8} kgs/m^3$, $\beta_2 = 61.38 \times 10^6\ Nm^{-2}deg^{-1}$, $T_0 = 293$K, $C_E = 383.1\ Jkg^{-1}K^{-1}$.

The remaining parameters are taken as

g_0 =1, $b_1 = 1$, c=0.5

The numerical investigation is carried out to examine the effects of thermal and diffusion phase lags on the axial displacement u_z, chemical potential P, temperature change T, and mass concentration C. In each case, one phase-lag parameter is kept fixed while the corresponding associated phase lag is varied. The results are plotted in the range $0 \leq r \leq 10$. The following four cases are considered:

a) $\tau_t = 0.08$, $\tau_q = 0$, 0.02 and 0.04

b) $\tau_q = 0.08$, τ_t= 0, 0.02 and 0.04

c) $\tau_\eta = 0.08$, $\tau_p = 0$, 0.02 and 0.04

d) τ_p=0.08, $\tau_\eta = 0$,0.02 and 0.04

In all figs, the solid line represents the zero phase-lag case, the small dashed line represents the phase-lag value 0.02, and the long dashed line with dots represents the phase-lag value 0.04.

Figs. 1–4 show the variation of axial displacement u_z with radial distance r for cases (a)–(d), respectively. Similarly, Figs. 5–8, 9–12, and 13–16 present the corresponding variations of chemical potential P, temperature change T, and mass concentration C, respectively, for the same four cases.

10.48047/jocaaa.2020.28.06.18

Fig. **1** shows the variation of axial displacement u_z with distance r for different values of τ_q, while keeping τ_t=0.08. For τ_q=0, the displacement shows a mild oscillatory variation with both positive and negative values. For τ_q=0.02, a sharp negative displacement occurs near r =0, followed by oscillatory behaviour as r increases. For τ_q=0.04, the displacement also varies in a wave-like manner, but with reduced amplitude compared with τ_q=0.02.

Fig. **2** presents the variation u_z with distance r for different values of τ_t, while keeping τ_q=0.08. For τ_t= =0, the displacement initially has a large negative value near the origin and then exhibits damped oscillations with increasing r. For τ_t=0.02, the response begins with a positive value and gradually changes into oscillatory behaviour. For τ_t=0.04, the displacement remains oscillatory, but the amplitude and phase differ from the other two cases.

Fig. **3** shows the variation of u_z with distance r for different values of τ_p keeping τ_η=0.08. It is observed that the axial displacement has large negative values near the loading surface for higher values of τ_p As r increases, the displacement gradually changes its trend and exhibits oscillatory behaviour. For τ_p=0, the variation is comparatively smooth with smaller amplitude, whereas for τ_p=0.02 and τ_p=0.04, the displacement shows stronger oscillations near the source region. Away from the loading surface, the amplitudes decrease and the curves tend to oscillate about the equilibrium position.

Fig. **4** presents u_z with distance r for distinct values of τ_η, while keeping τ_p=0.08. It is noticed that the displacement is strongly influenced near the source region and then changes in an oscillatory manner with increasing r. For τ_η=0, the displacement is initially negative, then increases and attains positive values in the intermediate region before oscillating about the equilibrium level. For τ_η=0.02, u_z attains a larger negative value near the origin and subsequently shows a rapid change with alternating positive and negative values. For τ_η=0.04, the displacement also begins with a negative value, but its amplitude and phase differ from the other two cases over the radial distance.

Fig.**5** depicts P with distance r for different values of τ_q while keeping τ_t=0.08. It is observed that P has a large positive value near the source region and decreases sharply as r increases. For τ_q=0, the curve decreases smoothly at first and then exhibits oscillatory behaviour. For τ_q=0.02, the chemical potential falls more rapidly and attains a larger negative value near r =2, followed by wave-like variations. For τ_q =0.04, the response also decreases initially and then oscillates with comparatively smaller amplitude.

Fig.**6** presents P with r for different values of τ_t, while keeping τ_q=0.08. In all cases, P starts with a high positive value near the origin and decreases rapidly with distance. For τ_t=0, the chemical potential reaches a negative minimum near the source region and then shows damped oscillations. For τ_t=0.02 and τ_t=0.04, similar oscillatory trends are observed, but with different amplitudes and phases. The comparison shows that variation in the temperature-gradient phase lag τ_t changes both the intensity and distribution of the chemical potential function in the plate.

Fig.**7** shows the variation of P with r for different values of τ_p while keeping τ_η=0.08. It is observed that P has a high positive value near the source region and decreases sharply with increasing r. For τ_p =0, the decrease is comparatively smooth, followed by small oscillations. For τ_p =0.02 and τ_p =0.04, the chemical potential decreases more rapidly near the origin and then exhibits oscillatory behaviour with different amplitudes. Away from the source region, all curves tend to oscillate about the zero level with reduced magnitude.

Fig.**8** displays P with r for different values of τ_η while keeping τ_p =0.08. It is observed that P starts with a large positive value near the source region and decreases sharply with increasing r. For τ_η==0, the chemical potential decreases smoothly at first, reaches a negative value, and then shows oscillatory behaviour. For τ_η=0.02, the curve attains a deeper negative value near r =2 and later exhibits wave-like variations with relatively higher amplitude. For τ_η=0.04, the decrease near the origin is comparatively less sharp than for τ_η=0.02, and the curve follows an oscillatory pattern with smaller amplitude in the later region.

10.48047/jocaaa.2020.28.06.18

Fig.**9** illustrates how T responds along the radial direction r when τ_q is varied and τ_t=0.08 is fixed. Near the source region, all curves begin with negative temperature change, indicating an initial drop in the thermal field. As r increases, the profiles recover from this negative region and develop wave-like fluctuations. The case τ_q =0 shows a gradual rise followed by moderate oscillations, whereas τ_q =0.02 produces a sharper recovery and a higher positive peak in the intermediate range. For τ_q =0.04, the curve also crosses into the positive region, but its oscillations are shifted in phase and remain comparatively restrained.

Fig.**10** presents the distribution of T with r for different values of τ_t with τ_q =0.08 . The thermal response is negative near the origin for all three cases, but the rate of recovery differs noticeably. When τ_t=0, the temperature rises comparatively smoothly and soon enters a positive oscillatory region. For τ_t=0.02, the negative zone extends over a larger radial distance before the curve gradually approaches positive values. In the case τ_t==0.04, the initial cooling effect is stronger, and the subsequent oscillations appear with a clear phase shift.

Fig.**11** depicts T with r for different values of τ_p with τ_η =0.08 fixed. The curves begin with a negative temperature change near the source region, showing an initial cooling effect. As the distance r increases, the temperature field gradually recovers and approaches the positive range. For τ_p =0, the recovery is smooth and the curve shows mild oscillations after crossing the zero level. For τ_p τp=0.02, the temperature rises more steadily and remains close to the zero level over a larger radial interval. For τ_p =0.04, the initial negative temperature change is more pronounced, followed by a delayed rise and small wave-like fluctuations.

Fig.**12** shows the variation of T along r for different values of $\tau_\eta$and τ_p =0.08 is kept fixed. The temperature response is strongly negative near the origin and then increases rapidly with distance. For τ_η =0, the curve rises smoothly and develops low-amplitude oscillations in the later region. For τ_η =0.02, the initial drop is sharper, but the curve reaches a comparatively higher positive value in the intermediate region. For τ_η =0.04, the response shows a delayed recovery from the negative zone and then follows an oscillatory path with a noticeable phase shift.

Fig.**13** describes the response of mass concentration C along the radial distance r for various values of τ_q, with τ_t =0.08 fixed. The concentration is initially large near the source and then falls rapidly as the radial distance increases. In case τ_q=0, the profile reduces smoothly and later shows mild fluctuations around the zero line. For τ_q=0.02, the concentration field exhibits a stronger initial response and a deeper fall in the intermediate region. When τ_q=0.04, the curve follows a similar decreasing tendency near the origin, but its later oscillations are shifted and comparatively moderated.

Fig.**14** describes the variation of C along the radial distance r for various values of τ_t, while τ_q=0.08 is fixed.. For τ_t=0, the concentration drops quickly and then settles into small oscillations. For τ_t=0.02, the decrease is slower in the initial range, and the curve maintains relatively higher values before entering the oscillatory region. In the case τ_t=0.04, the concentration starts from a comparatively larger value and decays with a noticeable phase shift in the subsequent wave pattern. Therefore, the temperature-gradient phase lag alters the diffusion response by changing the decay rate, amplitude, and phase of the concentration profile.

Fig.**15** presents C with r for distinct values of τ_p when τ_η=0.08 is maintained. For τ_p =0, the curve shows a smooth decay followed by small oscillations around the zero level. For τ_p =0.02, the concentration decreases more gradually and remains close to zero in the later region. For τ_p =0.04, the initial concentration is comparatively higher, followed by a sharper fall and a slightly shifted oscillatory pattern.

Fig.**16** illustrates C with r for distinct values of $\tau_\eta$with τ_p =0.08. Near the origin, the concentration is high for all cases and then decreases sharply with distance. For τ_η=0, the curve decays smoothly and later shows moderate oscillations. For τ_η=0.02, the initial concentration is larger and the curve exhibits a delayed decrease before entering the oscillatory region. For τ_η=0.04, the response starts with a comparatively high value and then follows a wave-like pattern with a noticeable phase shift.

10.48047/jocaaa.2020.28.06.18

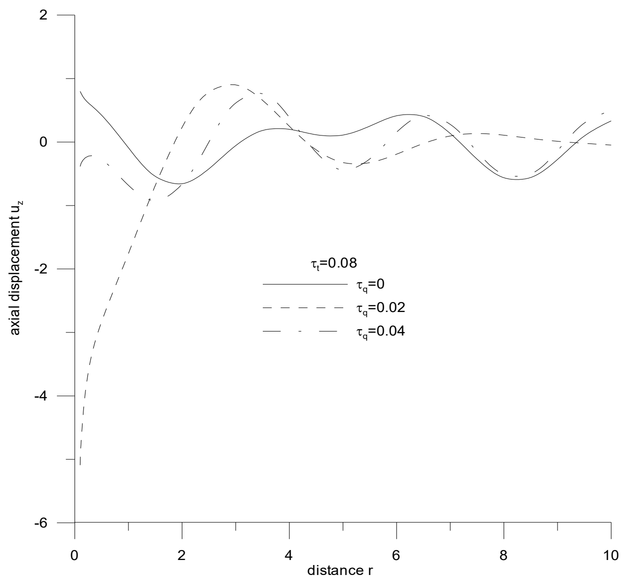

Fig.1.Variations of axial displacement u_z with distance r (case a)

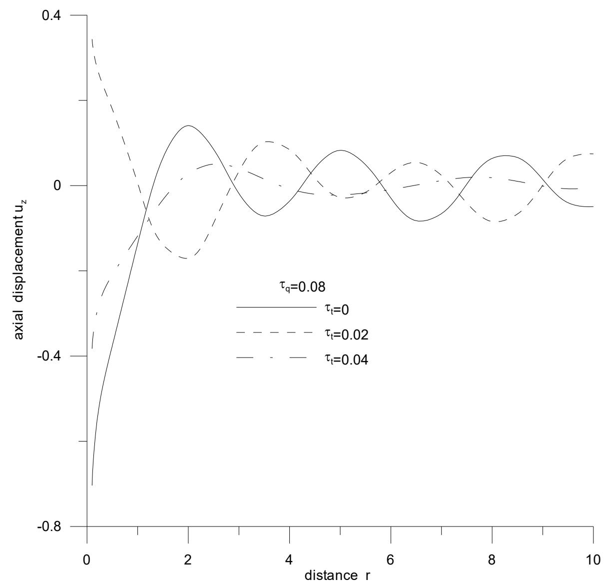

Fig.2.Variations of axial displacement u_z with distance r (case b)

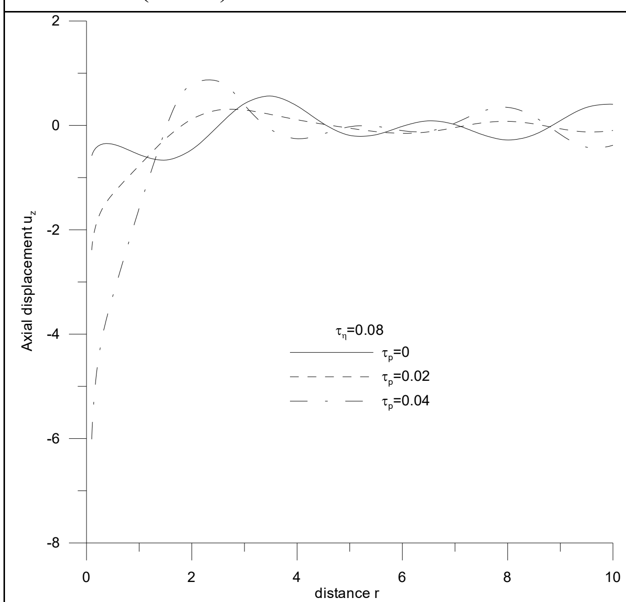

Fig.3.Variations of axial displacement u_z with distance r (case c)

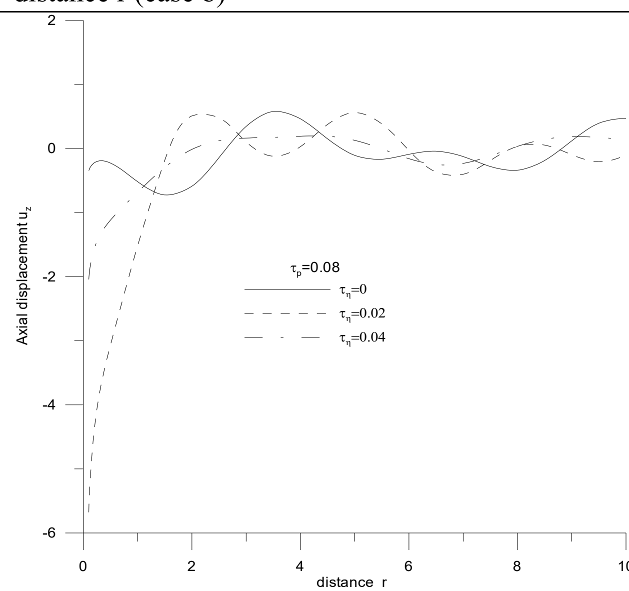

Fig.4.Variations of axial displacement u_z with distance r (case d)

10.48047/jocaaa.2020.28.06.18

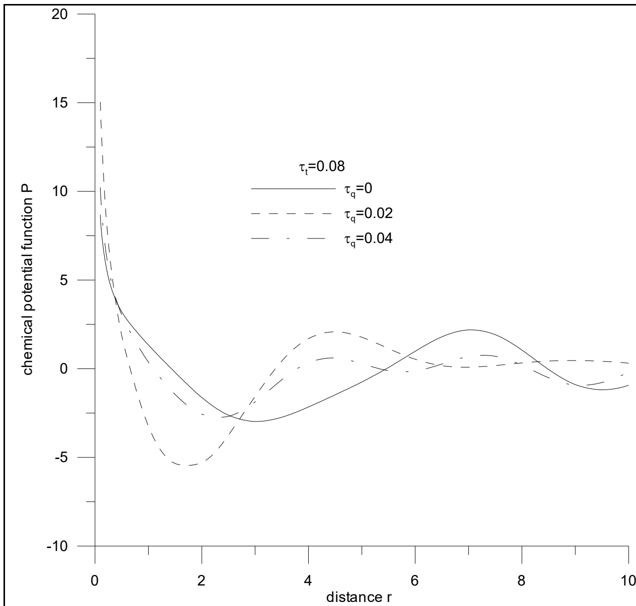

Fig.5.Variations of chemical potential function P with distance r (case a)

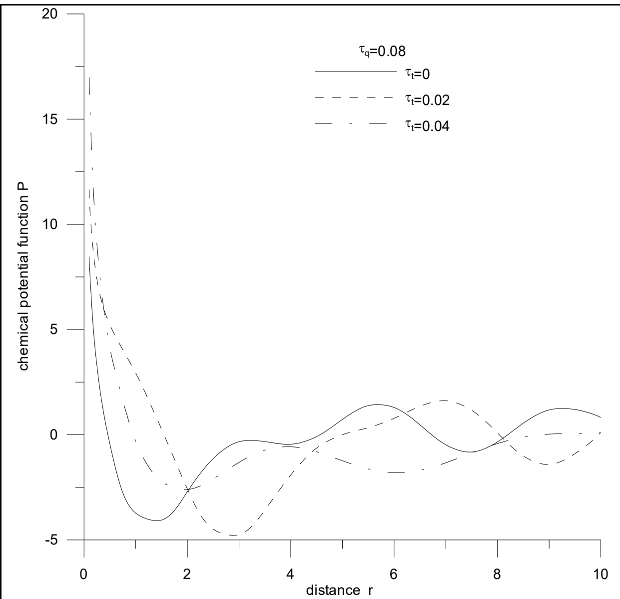

Fig.6.Variations of chemical potential function P with distance r (case b)

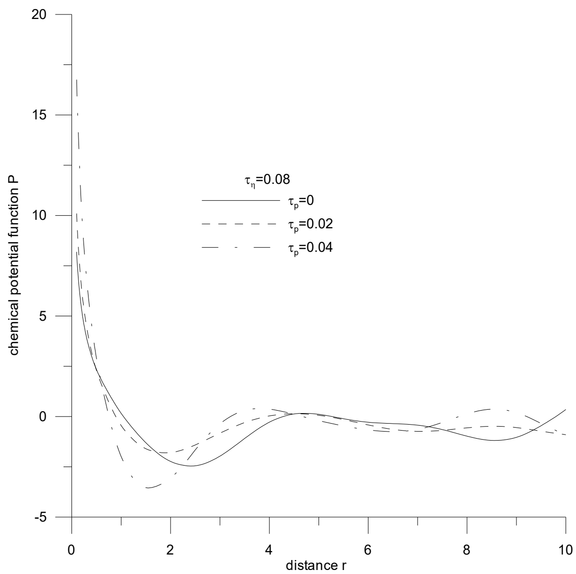

Fig.7 Variations of chemical potential function P with distance r (case c)

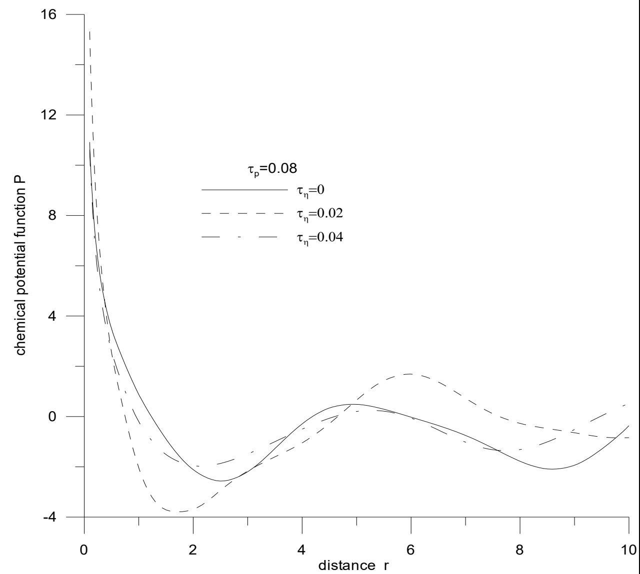

Fig.8 Variations of chemical potential function P with distance r (case d)

10.48047/jocaaa.2020.28.06.18

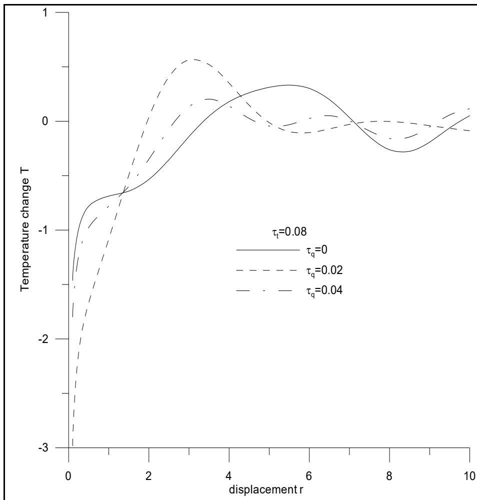

Fig.9.Variations of temperature change T with distance r (case a)

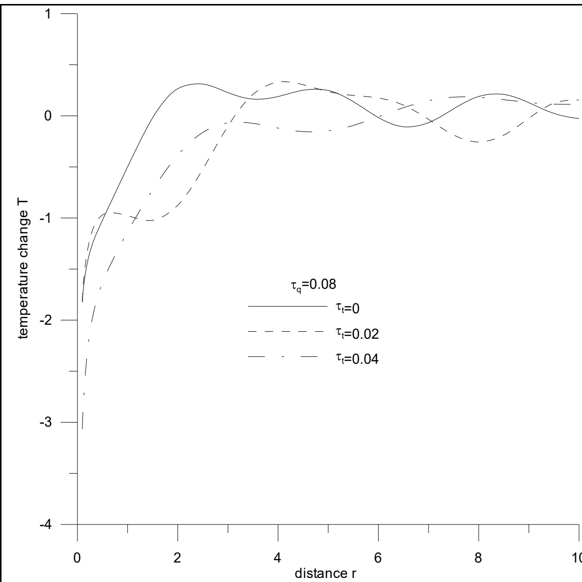

Fig.10.Variations of temperature change T with distance r (case b)

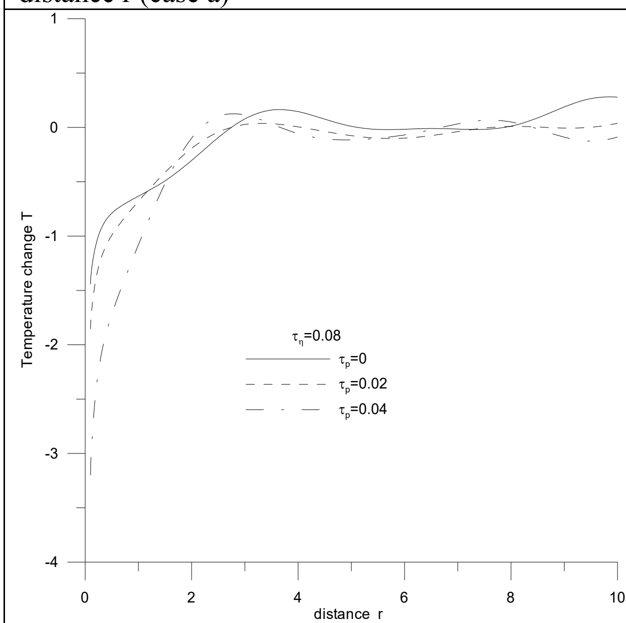

Fig.11.Variations of temperature change T with distance r (case c)

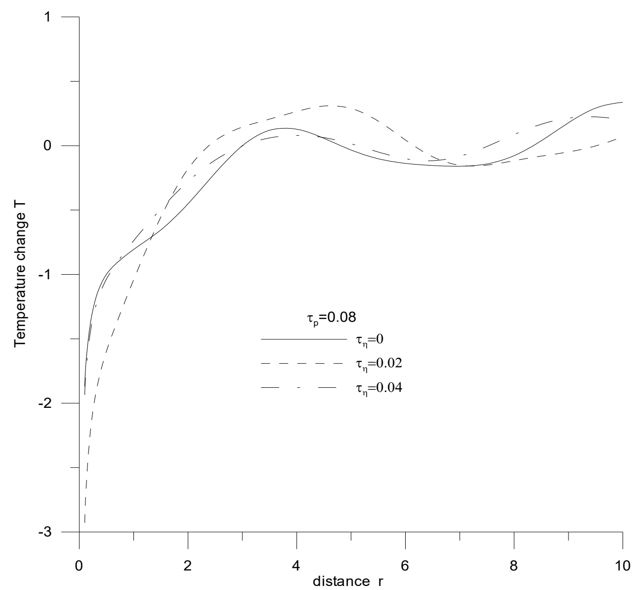

Fig.12.Variations of temperature change T with distance r (case d)

10.48047/jocaaa.2020.28.06.18

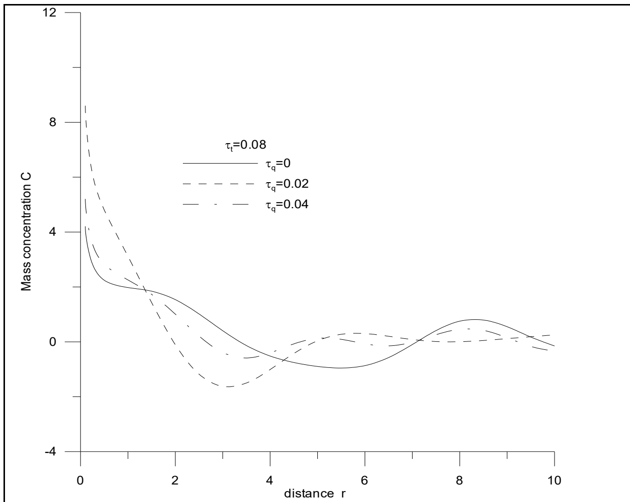

Fig.13.Variations of mass concentration C with distance r (case a)

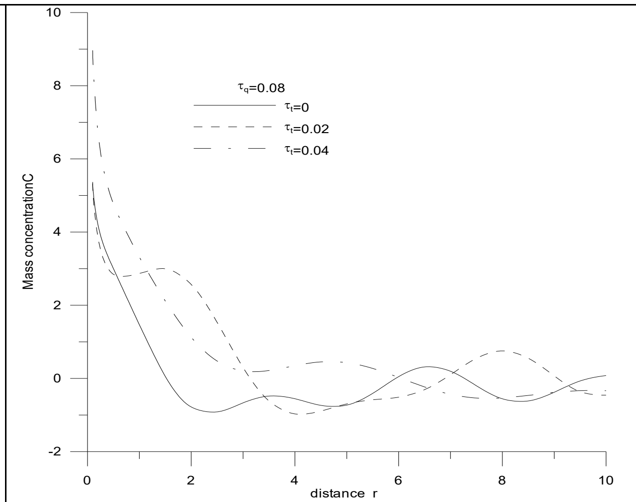

Fig.14.Variations of mass concentration C with distance r (case b)

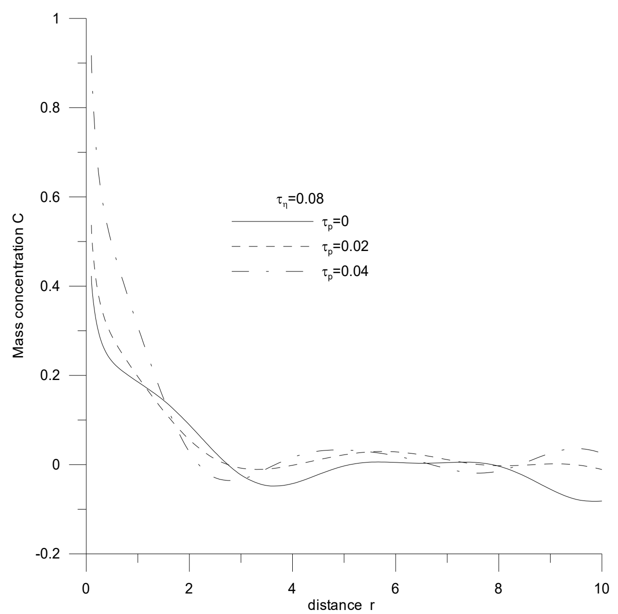

Fig.15.Variations of mass concentration C with distance r (case c)

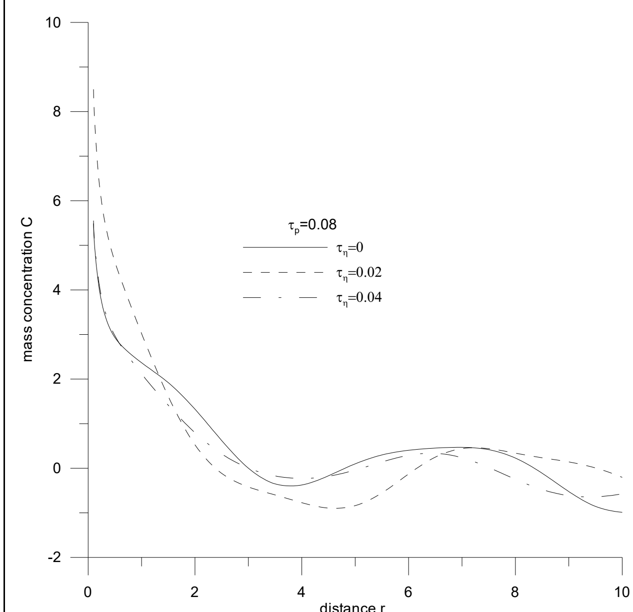

Fig.16.Variations of mass concentration C with distance r (case d)

8. Conclusion

The axisymmetric thermoelastic diffusion response of a homogeneous isotropic thick plate subjected to prescribed thermal and chemical potential sources has been investigated. The upper and lower surfaces are considered traction-free, with an axisymmetric heat supply and a radially expanding ring-type chemical potential source imposed on the plate. Using Laplace and Hankel transform techniques, the governing equations are solved in the transformed domain, and numerical inversion is applied to obtain the physical-domain response.

The numerical results indicate that the phase-lag parameters have a marked influence on all field variables. The axial displacement is highly sensitive near the source region, and its amplitude and phase change noticeably with variations in both thermal and diffusion phase lags. The chemical potential and

10.48047/jocaaa.2020.28.06.18

mass concentration show steep variations near the origin, followed by oscillatory behaviour along the radial direction. The temperature change is also strongly affected by the phase-lag parameters, confirming the coupled nature of heat transfer, deformation, and diffusion in the medium.

A comparison of different phase-lag cases shows that small changes in these parameters may lead to considerable differences in the magnitude and spatial distribution of the response. In particular, the diffusion phase-lag parameters significantly modify the chemical potential and mass concentration fields, highlighting the importance of including delayed mass-flux effects in generalized thermoelastic diffusion models.

The limiting cases derived from the present formulation show that several classical and generalized models can be recovered. The problem has potential applications in deformable solids subjected to thermo-diffusive sources, including geological media, advanced engineering materials, and industrial processes involving coupled heat and mass diffusion.

9. References

[1] Lord, H. W., & Shulman, Y. (1967). A generalized dynamical theory of thermoelasticity. *Journal of the Mechanics and Physics of Solids, 15*(5), 299–309. https://doi.org/10.1016/0022-5096(67)90024-5

[2] Green, A. E., & Lindsay, K. A. (1972). Thermoelasticity. *Journal of Elasticity, 2*, 1–7. https://doi.org/10.1007/BF00045689

[3] Tzou, D. Y. (1996). *Macro to Microscale Heat Transfer: The Lagging Behavior*. Taylor & Francis, Washington, DC, USA.

[4] Quintanilla, R., & Racke, R. (2006). A note on stability in dual-phase-lag heat conduction. *International Journal of Heat and Mass Transfer, 49*(7–8), 1209–1213.

[5] Rukolaine, A. S. (2014). Unphysical effects of the dual-phase-lag model of heat conduction. *International Journal of Heat and Mass Transfer, 78*, 58–63.

[6] Abdallah, I. A. (2009). Dual phase lag heat conduction and thermoelastic properties of a semi-infinite medium induced by ultrashort pulsed laser. *Progress in Physics, 3*, 60–63.

[7] Chou, Y., & Yang, R. J. (2009). Two-dimensional dual-phase-lag thermal behaviour in single-/multi-layer structures using CESE method. *International Journal of Heat and Mass Transfer, 52*, 239–249.

[8] Zhou, J., Zhang, Y., & Chen, J. K. (2009). An axisymmetric dual-phase-lag bioheat model for laser heating of living tissues. *International Journal of Thermal Sciences, 48*, 1477–1485.

[9] Liu, K. C., Cheng, P. J., & Wang, J. S. (2014). Analysis of thermal damage in a laser-irradiated based on non-Fourier model. *International Journal of Engineering and Technology, 6*(2), 132–135.

[10] Ying, X. H., & Yun, J. X. (2015). Time fractional dual-phase-lag heat conduction equation. *Chinese Physics B, 24*(3), 034401.

[11] Kumar, R., & Mukhopadhyay, S. (2010). Analysis of the effects of phase-lags on propagation of harmonic plane waves in thermoelastic media. *Computational Methods in Science and Technology, 16*(1), 19–28.

10.48047/jocaaa.2020.28.06.18

[12] Kumar, R., Chawla, V., & Abbas, I. A. (2012). Effect of viscosity on wave propagation in anisotropic thermoelastic medium with three-phase-lag model. *Theoretical and Applied Mechanics, 39*(4), 313–341.

[13] Sharma, S., Sharma, K., & Bhargava, R. R. (2013a). Effect of viscosity on wave propagation in anisotropic thermoelastic medium with Green–Naghdi theory of type II and type III. *Materials Physics and Mechanics, 16*(2), 144–158.

[14] Sharma, S., Sharma, K., & Bhargava, R. R. (2013b). Wave motion and representation of fundamental solution in electro-microstretch viscoelastic solids. *Materials Physics and Mechanics, 17*, 97–110.

[15] Sharma, K., & Kumar, P. (2013). Propagation of plane waves and fundamental solution in thermoviscoelastic medium with voids. *Journal of Thermal Stresses, 36*(2), 94–111.

[16] Sharma, K., & Bhargava, R. R. (2012). Propagation of thermoelastic plane waves at an imperfect boundary of thermal conducting viscous liquid/generalized thermoelastic solid. *Afrika Matematika*, 25(1-2), 81-102. https://doi.org/10.1007/s13370-012-0099-1

[17] Nowacki, W. (1974). Dynamical problems of thermo diffusion in solids I. *Bulletin de l'Académie Polonaise des Sciences, Série des Sciences Techniques, 22*, 55–64.

[18] Sherief, H. H., Saleh, H., & Hamza, F. (2004). The theory of generalized thermoelastic diffusion. *International Journal of Engineering Science, 42*, 591–608.

[19] Kumar, R., & Kansal, T. (2008). Propagation of Lamb waves in transversely isotropic thermoelastic diffusion plate. *International Journal of Solids and Structures, 45*(22–23), 5890–5913.

[20] Sharma, K. (2010). Boundary value problems in generalized thermodiffusive elastic medium. *Journal of Solid Mechanics, 2*(5), 348–362.

[21] Sharma,K. (2011). Analysis of deformation due to inclined load in generalized thermodiffusive elastic medium. *International Journal of Engineering, Science and Technology, 3*(2), 117–129.

[22] Sharma, N., Kumar, R., & Ram, P. (2012). Interactions of generalized thermoelastic diffusion due to inclined load. *International Journal of Emerging Trends in Engineering and Development, 5*(2), 583–600.

[23] Atwa, S. Y. (2013). Generalized thermoelastic diffusion with effect of fractional parameter on plane waves temperature-dependent elastic medium. *Journal of Materials and Chemical Engineering, 1*(2), 55–74.

[24] Bhattacharya, D., & Kanoria, M. (2014). The influence of two-temperature generalized thermoelastic diffusion inside a spherical shell. *International Journal of Engineering and Technical Research, 2*(5), 151–159.

[25] Kumar, R., & Gupta, V. (2014). Plane wave propagation in an anisotropic dual-phase-lag thermoelastic diffusion medium. *Multidiscipline Modeling in Materials and Structures, 10*(4), 562–592.

10.48047/jocaaa.2020.28.06.18

[26] Tripathi, J. J., Kedar, G. D., & Deshmukh, K. C. (2015). Generalized thermoelastic diffusion problem in a thick circular plate with axisymmetric heat supply. *Acta Mechanica, 226*(7), 2121–2134.

[27] Li, C., Guo, H., Tian, X., & Tian, X. (2017). Transient response for a half-space with variable thermal conductivity and diffusivity under thermal and chemical shock. *Journal of Thermal Stresses, 40*(3), 389–401. https://doi.org/10.1080/01495739.2016.1218745

[28] Kumar, R., Miglani, A., & Rani, R. (2018). A two-dimensional axisymmetric thermoelastic diffusion problem of micropolar porous circular plate with dual phase lag model. *Mechanics and Mechanical Engineering, 22*(4), 1389–1406. https://doi.org/10.2478/mme-2018-0109

[29] Xue, Z. N., Yu, Y. J., Li, X. Y., & Tian, X. G. (2019). Study of a generalized thermoelastic diffusion bi-layered structure with variable thermal conductivity and diffusivity. *Waves in Random and Complex Media, 29*(1), 34–53. https://doi.org/10.1080/17455030.2017.1397810

[30] Tokovyy, Y. V. (2019). Solutions of axisymmetric problems of elasticity and thermoelasticity for an inhomogeneous space and a half-space. *Journal of Mathematical Sciences, 240*, 86–97. https://doi.org/10.1007/s10958-019-04337-3

[31] Gaver, D. P. (1966). Observing stochastic processes and approximate transform inversion. *Operations Research, 14*, 444–459.

[32] Stehfest, H. (1970). Algorithm 368: Numerical inversion of Laplace transforms. *Communications of the ACM, 13(1)*, 47–49. https://doi.org/10.1145/361953.361969

[33] Stehfest, H. (1970). Remark on Algorithm 368: Numerical inversion of Laplace transforms. *Communications of the ACM, 13(10)*, 624. https://doi.org/10.1145/355598.362787

[34] Press, W. H., Flannery, B. P., Teukolsky, S. A., & Vetterling, W. A. (1986). *Numerical Recipes: The Art of Scientific Computing*. Cambridge University Press, Cambridge.

[35] Dhaliwal, R. S., & Singh, A. (1980). *Dynamic Coupled Thermoelasticity*. Hindustan Publishing Corporation, New Delhi, India.